Temporal Deep Learning Assisted UAV Communication Channel Model For Application in EH-MIMO-NOMA Set-up

Aradhana Misra, Manash Pratim Sarma, Kandarpa Kumar Sarma, and Nikos Mastorakis

***Abstract*—The radio frequency (RF) spectrum is crucial for effective deployment of unmanned aerial vehicle (UAV). The unpredictability of the communication channel restricts link reliability and quality of service (QoS) of the UAV's deployment. Though several approaches have already been reported to model the communication channel of the UAV, the necessity of optimal spectrum utilization, better link reliability and QoS requires that new methods be explored for effective representations of propagation variations and path gains present in the UAV flight profile. Here, we report the design of a learning aided model of the UAV communication channel. We use a deep learning (DL) based method which relies upon different taped delay line (TDL) driven layers of gated functions implanted as part of specifically designed networks for capturing the channel state information (CSI) of the propagation medium. The key part is the use of context processing and recovery layers formed by these TDL driven gated function structures which provide performance enhancements. The proposed model is trained and tested with synthetic and actual data and is supported by energy harvesting attributes. It has been found to be effective in modeling UAV channels while deployed with multi input multi output (MIMO) and non-orthogonal multi access (NOMA) set-up in urban areas and in platforms moving with a maximum velocity of 60 kmph.**

***Index Terms*—AR, ARMA, artificial neural network, channel modeling, deep learning, energy harvesting, LSTM, NAR, NARMA, UAV.**

I. Introduction

THE application of the unmanned aerial vehicle (UAV), popularly called drone, has been increasing at unprecedented scale and has been adopted as a tool in many domains of human activity [1], [2]. More commonly UAVs are being applied for agriculture [3], [4], a range of surveillance activities, extension of range of wireless communication systems, delivery of items [1]–[4] and more lately to assist people engaged in fighting pandemic situations due to COVID-19. These programmable platforms can assist medical professionals by providing preliminary diagnostics, drug and food delivery in quarantine centers, hospitals to name a few and can also be used for sterilization, de-contamination and cleanliness drives in hospitals, residential blocks, neighborhoods etc. Further, drones are readily available aids for support staff and security agencies in large scale screening and monitoring, ensuring social distancing, quarantining and treatment of the patients, traffic monitoring etc. The ability of a UAV to supply essential aid and support in out-of-the-reach locations at crucial times have given birth to delivery drones. This is very much relevant to fight epidemics and prevent large scale fatality. Especially in cases of virus related medical emergencies, people at quarantine centers may receive food and medicine through drones. Robots and UAVs provide a layer of safety, greater reach and efficiency in crisis situations which make them ideal to play a complementary supplementary role to the medical fraternity. UAVs are vital for risk assessment, developing contingency plans, initiating response where human help is less likely and provide initial support.

The control of the drone is carried out using specified slots in the radio frequency (RF) spectrum around 840.5–845 MHz, 1430–1444 MHz, and 2408–2440 MHz [5]. Due to the unprecedented growth in mobile and wireless communication technologies in recent times, the RF spectrum has already become overcrowded which threatens the UAV control and link channels. It makes imperative to have resilient means of ensuring link reliability and quality of service (QoS). Lately it has become a norm to accept that a crucial aspect related to link reliability and QoS is associated with the development of methods that have certain situational awareness and are adaptive with the variations of the surrounding environment [6]. Attributes like adaptive processing and situation awareness are best exemplified by artificial intelligence (AI) [7] and learning based tools. These have the ability to learn from the surroundings, track the variations in the environment and make sufficient adjustments in the process flow so that proper recovery of data and generation of relevant response becomes efficient [8].

The UAV channel model provides ample of scope of application of AI due to its inherent uncertainty. Similarly, learning aided (LA) approaches enhance the quality of estimation and contribute towards better link reliability. In terms of tools, several data driven (DD) and machine learning (ML) techniques are available to make UAV channel model more suitable for real time conditions and achieve optimal processing. Traditionally, UAV models fall in two categories. The first is the deterministic model and the second category is the statistical model. Deterministic models are known for

Manuscript received March 22, 2021; revised July 22, 2021; approved for publication by Osman Yağan, Guest Editor, September 2, 2021.

A. Misra, M. p. Sarma, and K. K. Sarma are with the Department of Electronics and Communication Engineering, Gauhati University, Guwahati-781014, Assam, India, email: {aradhana.misra, mpsarma}@gauhati.ac.in, kandarpaks@gmail.com.

N. Mastorakis is with Technical University of Sofia, Sofia, Kliment Ohridski 8, Bulgaria, email: mastor@tu-sofia.bg.

K. K. Sarma is the corresponding author.

Digital Object Identifier: 10.23919/JCN.2021.000045

1229-2370/22/$10.00 © 2022 KICS

their accuracy which is derived from a strong dependence on actual data. Actual data from field conditions are collected but require extensive experimental work and tedious analysis. In the deterministic model, environmental objects are assigned larger dimensions compared to the wavelength. The clutter generated from environmental objects are placed in the certain layouts. There is no scope for compensating the scattering due to diffusion. The database of the details related to terrain topography, electrical parameters of natural and human created obstructions etc determine the accuracy of the model. This makes the deterministic models less popular. The ray-tracing model [9], [10] and finite-difference time domain method (FDTD) [11] model are examples of UAV deterministic model. Elements of non-geometrical statistical model (NGSM) and geometry-based statistical model (GBSM) formulate the statistical model [12]. Commonly used tapped delay line (TDL) model and multipath models with line of sight (LOS) and non-LOS (NLOS) components covering ground reflection, multi-path elements etc constitute the vital organs of the UAV statistical model. These are not dependent much on actual data, work with synthetic content and can be created using computational approaches.

Despite the time-tested virtues of the traditional models, certain aspects like traffic congestion, location specific services, dynamic positioning, interference management, fading due to Doppler effect, shadowing etc require that ML be integrated to the UAV channel modeling [13]. These issues have been instrumental in the execution of a number of studies which have reported the use of a host of ML and data driven approaches for UAV communication channel modeling [14]–[22]. The key consideration of these works have been the use of ML and deep learning (DL) based approaches which are known for their ability to adapt and optimize as per the surrounding wireless profile and requirements, learn from the surroundings, retain the learning and use it subsequently. Such aspects have made ML/DL approaches popular and have become integral elements of 5G wireless communication. ML/DL tools are able to extract relevant information for continuous flow of data and provide relevant decision making support to facilitate effective use of UAVs for a range of applications. A key factor related to the generation of better reliability using the ML/DL approaches is linked to their ability to capture the time-dependent variations in the signal and account for all states of the channel state information (CSI). For that subtle changes in the architecture are required because traditional ML systems are not intended to perform such tasks. Earlier, among the ML tools, artificial neural networks (ANN) like time delay neural network (TDNN), recurrent neural network (RNN) etc have been preferred though they continue to be used as benchmark techniques. Lately, gated function based DL methods have started to gain popularity in UAV channel modeling. These techniques have been designed to develop approaches as part of DL techniques enabling them to capture the context and different dependencies. Two fundamental factors are behind the shift of preference towards these architectures. First, is the ability of these learning based gated functions to execute dynamic control while associating past content with the current state at each instant of time. The second factor is the ability of these gated functions to prevent disruption in learning which is caused by the vanishing or exploding gradient problem observed in traditional dynamic ANN [23]. These two factors are also vital in the proper modeling of the UAV channel.

A. Related Work

Some of the relevant literature are as in [24]–[30]. In [24], an approach of short-term traffic forecasting with spatial temporal correlation in a hybrid deep learning framework is discussed. Extreme traffic conditions using DL methods are discussed in [25]. A gated approach based on long short term memory (LSTM) cells for short term traffic prediction is discussed in [26]. In [27], authors report the use of a bidirectional and unidirectional LSTM RNNs for traffic speed prediction. High order graph convolutional RNNs have been applied for network scale traffic prediction in [28]. Mobility predictions for IoT devices using gated functions have been discussed in [29]. Prediction of user mobility has been a topic of a thesis as reported in [30]. In all these cases, the gated functions have shown appreciable performance while dealing with a diverse range of predictions involving mobility. Use of a host of ML and data driven approaches for UAV communication channel modeling have been reported in [14]–[22]. In [37], authors have reported the application of a deep learning based approach to model path loss on fixed wireless access techniques in suburban scenarios. In [38] and [39], learning aided approaches for proper utilization of the UAV channel have been reported. Despite the reported use of several learning based approaches for UAV channel modeling, there are opportunities for obtaining performance improvements and optimal computation if the input feed mechanisms are expanded with tapped delay line (TDL) [31], [32] blocks and configuring gated functions in innovative combinations to facilitate detailed feature learning, missing content recovery, tracking time variations and preserving context of the processed content. The resultant signal becomes context and content rich and contributes towards better reliability while applied for UAV channel modeling.

B. Contribution

In the backdrop of evolving capabilities of the innovative combinations of gated functions with a few known DL/ML architectures here we discuss the design of a learning based mechanism designed specifically for the UAV communication channel modeling. The approach is based on two gated functions namely vanilla recurrent cell (VRC) and LSTM integrated with TDL blocks in the input feed line. These are called TDL-VRC and TDL-LSTM. Together with an auto-encoder, the TDL-VRC and TDL-LSTM blocks are used to formulate separate layers for processing and tracking the variations of the UAV communication channel. Specifically, these innovative gated functions are used to formulate contextual processing and denoising layer (L1), feature learning layer (L2), recovery layer (L3) and discrimination layer (L4). Each of these layers have specific roles to play and are held at pre-trained levels using supervised gradient descent (SGD) BP algorithm. The training is carried out using data accumulated

from Jakes [32] wireless multipath fading model and actual measurements in situations with NLOS and LOS components. The performance of the proposed approach has been judged in terms of signal to noise (SNR) gain, capacity generated, bit error rate (BER), channel tracking etc and compared with traditional ANN and statistical methods like decision feedback equalizer (DFE) [36], delayed decision feedback estimator (DDFE) [36] (in least square (LS) and minimum mean square error (MMSE) senses). The experimental samples include NLOS and LOS conditions with Doppler shift upto 60 Kmph. Antenna diversity achieved with 2×2 structures are used to ascertain the benefits of such a system to provide high data rate connectivity. Further, the work considers energy harvesting (EH) as an attribute for range and battery life extension of the UAV Specific channel considerations and device level implementation have been carried out and experimentally verified. The work has been tested in multi input multi output (MIMO) and non-orthogonal multi access (NOMA) setups which are commonly observed in urban areas. Experimental results demonstrate significant performance improvements in terms of SNR path gain and capacity (bit/s/Hz) compared to certain benchmark techniques.

The novelty of the work is the use of TDL-VRC and TDL-LSTM cells along with an auto-encoder to an innovative DL structure constituted by contextual processing and denoising layer (L1), feature learning layer (L2), recovery layer (L3) and discrimination layer (L4) to track variations of the UAV communication channel, estimate path gains while using MIMO diversity and NOMA for capacity and coverage improvements and demonstration of extension of the UAV battery life with the use of an energy harvesting mechanism.

The rest of the paper is organized as follows. Section II describes the proposed model in details. Experimental results and related discussion have been covered in Section III. The work and the outcomes are summarized in Section IV.

II. Proposed Approach

Here we discuss the proposed approach. First, we describe in brief the basic concepts of TDL-VRC, TDL-LSTM and the composition of different layers. We provide the basic mathematical approaches related to the responses generated by these blocks and outline the key features of the UAV channel.

A. TDL-VRC

The vanilla recurrent cell (VRC) is a type of recurrent processing block which generates the output using present input and past or hidden states to show time-dependent behavior. It is able to track variations in time. Our proposed TDL-VRC has a delayed feed mechanism in the input. It helps to retain the context, temporal attributes and facilitate content rich processing. Fig. 1 shows a TDL-VRC.

Let $X(t)$ be the applied signal and $h(t-1)$ be the state vector of previous stage. With tapped delays, the signal at the input stage is $X(t)W_1 + X(t)W_2$ with W_1 and W_2 being the weights with the input and delayed feed lines, respectively.

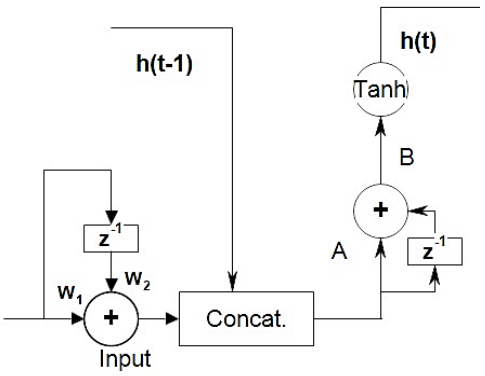

Fig. 1. TDL-VRC.

At point A, the signal shall be:

$$X_1(t) = Concat.\{(X(t)W_1 + X(t)W_2, h(t-1))\}, \quad (1)$$

where $Concat.(.)$ is a function that concatenates $h(t-1)$ after $X(t)$.

At point B, the sequence shall be:

$$X_2(t) = \mathbf{W} \times \{X_1(t) + X_1(t-1)\}, \quad (2)$$

where $\mathbf{W}$ is a weight term. The output of the system shall be

$$h(t) = tanh\ \{X_2(t) + b\}, \quad (3)$$

where b is a bias term.

B. TDL-LSTM

The LSTM is one of the popular gated functions which has received considerable attention in recent times due to its ability to deal with time series, sequencing and related domains. With known time gaps or lags in the input, the LSTM is able to do classification, prediction, and process time series sequences. Despite sampled feed, the output shows no influence of the left portions of the patterns on the LSTM's response and is able to capture long term dependencies and the context. Further, it is free from the vanishing gradient problem and training is sustained without getting stuck in the local minima problem as observed in TDNN or RNN [8]. In the present case, we integrate a TDL in the input feed line of the LSTM to enhance it ability to retain time dependent relevant segments and process temporal content of the patterns. The TDL expands the LSTM's ability to capture the contextual portion more effectively which is essential for a time varying phenomenon like the UAV wireless communication channel. Fig. 2 shows the diagram of the TDL-LSTM unit which is used to build the proposed DL based UAV model.

Let $X(t)$ be the input, $C(t-1)$ is inclusion in memory cell from previous state and $h(t-1)$ be the past state of the context vector. At A, the signal shall be:

$$X_1(t) = \{X(t)W_{01} + X(t-1)W_{02}\} \times \mathbf{W}_1, \quad (4)$$

where W_{01} and W_{02} are weights with the input and delayed feed lines, respectively, and $\mathbf{W}_1$ is the connectionist weight. Similarly,

$$f_1(t) = sign.\ [\{X_1(t) + \mathbf{U}_1 h(t-1)\} \times \mathbf{W}_2 + b_1], \quad (5)$$

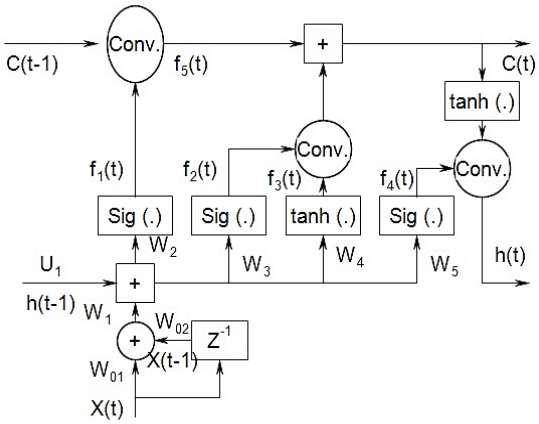

Fig. 2. LSTM unit with TDL in the input.

where $\mathbf{U}_1$ is the weight associated with the feed of the previous state vector $h(t-1)$, b_1 is a bias and $\mathbf{W}_2$ is a connectionist weight. Further,

$$f_2(t) = sign.\ [\{X_1(t) + \mathbf{U}_1 h(t-1)\} \times \mathbf{W}_3 + b_2], \quad (6)$$

where b_2 is a bias and $\mathbf{W}_3$ is a connectionist weight. Also,

$$f_3(t) = tanh\ [\{X_1(t) + \mathbf{U}_1 h(t-1)\} \times \mathbf{W}_4 + b_3], \quad (7)$$

where b_3 is a bias and $\mathbf{W}_4$ is a connectionist weight. Again,

$$f_4(t) = sign.\ [\{X_1(t) + \mathbf{U}_1 h(t-1)\} \times \mathbf{W}_5 + b_4], \quad (8)$$

where b_4 is a bias and $\mathbf{W}_5$ is a connectionist weight. This gives

$$f_5(t) = f_1(t)\ *\ C(t-1), \quad (9)$$

such that

$$C(t) = f_5(t) + f_2(t)\ *\ f_3(t), \quad (10)$$

and

$$h(t) = f_4(t)\ *\ tanh\ C(t)), \quad (11)$$

where $sign.(.)$ and $tanh(.)$ are $signum$ and $tanh$ activation functions, respectively.

C. UAV Channel

The UAV channel has both LOS and NLOS components and suffers extensive multipath fading. Further, the channel generates Doppler related fluctuations due to variations in position and movement at certain speeds. The multipath fading characteristics observed in a UAV wireless channel with NLOS elements are represented by Rayleigh statistics and the LOS elements are accounted by the Rician distribution. Fig. 3 depicts a UAV channel. It has multiple segments namely from the source to the UAV and from the UAV to the destination. In both these two segments, there are large and small scale fading. The UAV channel can be described using large scale path gain ($h_{LS}(,)$) and small scale channel components ($h_{SS}(,)$) [33]. Using a truncated discrete filter block, these two components are described as below:

$$h_{LS}(\tau, t) = \sum_{k=1}^{N_{LS}(t)} \alpha_k^{LS}(t)\delta(\tau - \tau_k^{LS}(t)), \quad (12)$$

and

$$h_{SS}(\tau, t) = \sum_{k=1}^{N_{SS}(t)} \alpha_k^{SS}(t)\delta(\tau - \tau_k^{SS}(t)), \quad (13)$$

such that

$$h(\tau, t) = h_{LS}(\tau, t) + h_{SS}(\tau, t), \quad (14)$$

where α_k is the magnitude of the signal attenuation, N_{LS} and N_{SS} are the length of the linear filters used for defining large and small scale effects respectively and τ_k is the delay suffered by the signal during transmission. So if two channel elements of $h(\tau, t)$ are considered between the source and the UAV ($h_{SU}(.)$) and the UAV and destination ($h_{UD}(.)$), for a transmitted signal $X_T(t)$, the received signal shall be

$$X_R(t) = \{h_{SU}(t)\ *\ X_T(t)\}\ *\ h_{UD}(t) + n_o, \quad (15)$$

where n_o is additive white Gaussian noise (AWGN). In this work we have concentrated on the multi input multi output (MIMO) channel of which a 2×2 set-up for UAV communication is considered. Further, the work is extended to a NOMA situation where the MIMO contributes to enhance diversity gain. The MIMO-NOMA set-up helps to maintain the link reliability, prevent outage in low coverage regions and is experimented with both LOS and NLOS components. The path gains are estimated using the proposed approach. Fig. 4 shows the path gain of 2×2 MIMO channel considered for the work.

D. Design of a Recovery Layer (L3)

An important portion of the work is the design of a novel recovery layer which uses a combination of TDL-VRC and TDL-LSTM blocks to deal with sparse values. The recovery layer substitutes values of channel gains lost while passing through edge of the coverage regions, temporary and sudden lost of link, excessive fading, power fluctuations in base stations, sudden breakdown, system reset, service breaks etc. These breaks generate lost states in the input sequence. With lost states, the output generated will also contain certain missing values. Further, if the missing states remain as nulls, it will contribute to the generation of more null states. Also, if these missing states are replaced by other predefined values, unreliable outputs will be generated. Further, if pre-defined values are applied as substitutes, it will result in biased output. Hence, regeneration of missing values using sparse inputs through a sequence of adaptive iterations carried out by the recovery layer is essential to ensure reliable substitution of the missing states. During modeling and estimation, the lost values are recovered by this layer. It carries out a series of iterations based on (error) back propagation (BP) algorithm and regenerates the missing or sparse samples. These samples ensure that the continuity of the CSI values are not lost so that the link reliability improves. It contributes towards better CSI estimation which is crucial for achieving higher throughput and better QoS. The key aspect of the working of the recovery layer is the fact that hybrid cells formed by TDL-VRC and TDL-LSTM in a sequence use past values of the context vector $h(t)$ and input $X(t)$ to generate present and future values of the output. The combined working of the TDL-VRC

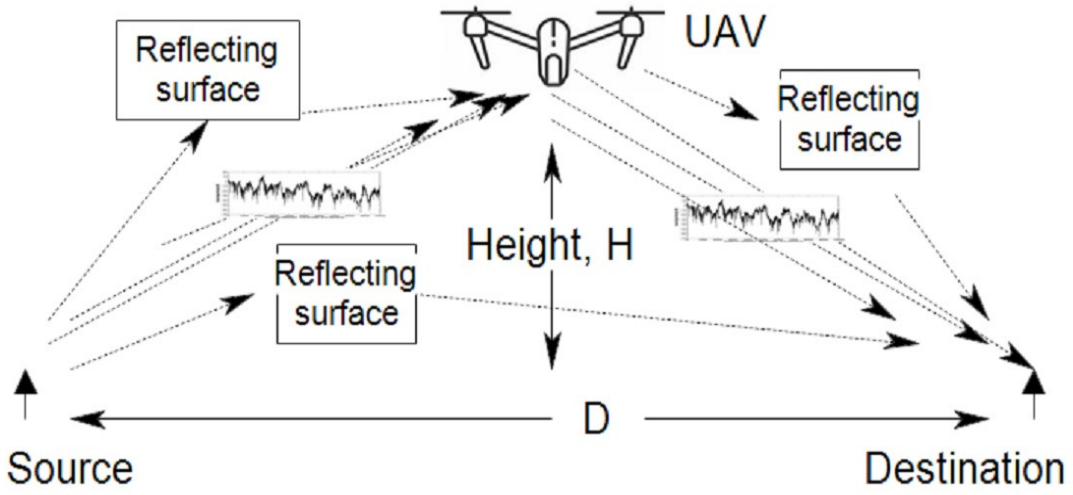

Fig. 3. UAV wireless communication channel.

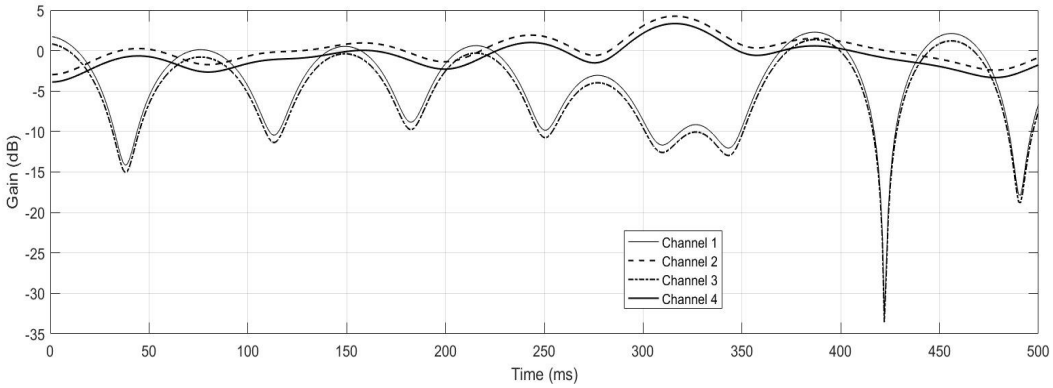

Fig. 4. Path gains of a 2 × 2 MIMO UAV channel.

and TDL-LSTM cells enable generation of lost values of the CSI. It prevents sparsity from disrupting the training of the network blocks and the complete system. The ability of the LSTM to retain long term dependencies and process time-dependent samples effectively is crucial in this case. RNNs have the ability of modeling non-linearities in input patters. In that same line, the VRC is effective in capturing the non-linear elements in the input feed. But the difficulties of the RNN related to its vanishing or expanding gradient problem puts restrains on its ability to deal with time varying patterns. This is also relevant with a layer of VRC. The LSTMs are effective in dealing with the vanishing or expanding gradient problem [8]. Therefore a combination of VRC and LSTM shall enable modeling of non-linearities present in the input and effectively deal with the vanishing or expanding gradient problem while efficiently processing the normal elements of the wave. The resultant training or learning is fast and efficient. Also, the presence of VRC and LSTM guarantee that no null states or zero values are generated and the training attains the destined target. Further, the presence of the TDL block reinforces the temporal processing capabilities.

Fig. 5 shows the layout of the recovery layer where $h(.)$ is a state vector and $X(.)$ is an input. The expressions of responses generated by this recovery layer are as outlined below: At point A:

$$Y(t-1)_{11}(t)=TDL\_VRC\{X(t-1)+h(t-1)\}, \quad (16)$$

$$Y(t-1)_{12}(t)=TDL\_LSTM\{X(t-1)+h(t-1)\}, \quad (17)$$

$$Y(t-1)=Y(t-1)_{11}(t)+Y(t-1)_{12}(t). \quad (18)$$

At point B:

$$Y(t)_{11}(t)=TDL\_VRC\{Y(t-1)+x(t)\}, \quad (19)$$

$$Y(t)_{12}(t)=TDL\_LSTM\{Y(t-1)+X(t)\}, \quad (20)$$

$$Y(t)=Y(t)_{11}(t)+Y(t)_{12}(t). \quad (21)$$

At point C:

$$Y(t+1)_{11}(t)=TDL\_VRC\{Y(t)+X(t+1)\}, \quad (22)$$

$$Y(t+1)_{12}(t)=TDL\_LSTM\{Y(t)+X(t+1)\}, \quad (23)$$

$$Y(t+1)=Y(t+1)_{11}(t)+Y(t+1)_{12}(t). \quad (24)$$

For the working of the L1 layer, peak value of the input signal is detected. A threshold fixed at 5% of the peak value is used to determine the sparse or missing states of the CSI. Under slow fading conditions, at the input of the L1 layer, from a P sized sequence, if k values are found to be sparse

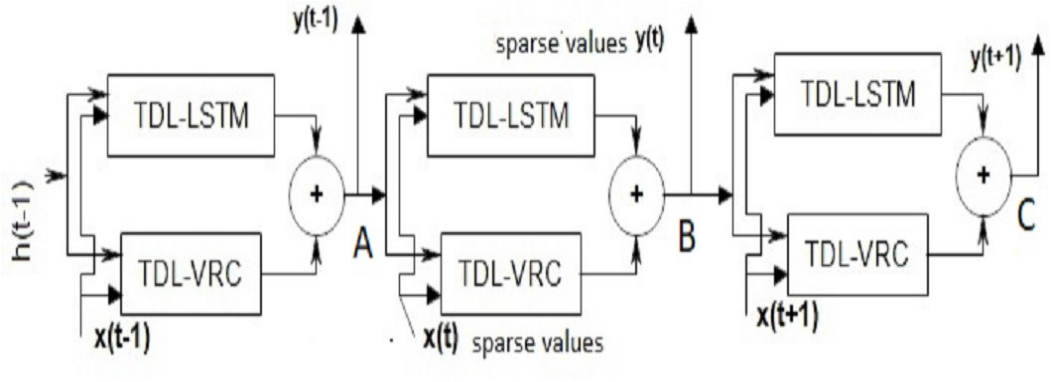

Fig. 5. Recovery layer using a combination of TDL-VRC and TDL-LSTM blocks.

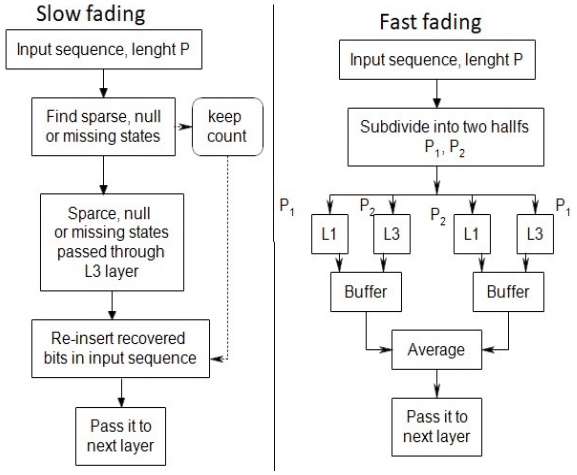

Fig. 6. Working of the recovery layer.

or with missing states, these are passed through the recovery layer, processed and added along with the output of the L1 layer. Under fast fading conditions, two halfs of the P sized sequences are made. One segment is passed through the L1 layer and the other half passed through the L3 layer. After processing both segments are combined and held in a buffer of size P. The above is repeated with the other sequence and the resultant segments are combined and stored in a buffer. An average of the sequences in the buffer are obtained and passed on to the next layer. This is summarized in Fig. 6.

E. Contextual Processing using Auto-Encoder Layer (L1)

This layer performs de-noising, feature learning, encoding-decoding and context capturing. These processes are important to capture the fast changing patterns observed in the UAV channel. Also the relevant features necessary for proper modeling of the UAV channel are also learnt by this layer. Further, channel noise is a detrimental effect observed in all communication signals. Auto-encoders are excellent de-noising systems [8]. Hence, removal of unwanted components from the signal and retaining the contributing aspects of the feed is ensured by this layer. It is formed by conventional VRCs and has a delayed feed line along with the present input. Further, this delayed feed of the inputs enables the front end of the block to process the temporal attributes of the signal. Simultaneously, as preceding cells feed the subsequent cell and circulate the contextual and related content, it generates a sequence of related samples from initial feeds from which noise and common mode components are removed. This sequence is rich in features of the UAV channel and encapsulates the content richness necessary for efficient processing in the subsequent stages. In a communication medium, the samples are intricately related. These intricate associations are needed to be captured and related with subsequent stages of processing. This sequential feed of the processing block generated by preceding unit and passing it on to the next cell ensures the learning of the intricate associations between the signal samples. It facilitates fast and correct learning. Here, only VRC cells are used to lower computational and design complexities. Moreover, the vanishing or expanding gradient problem is not observed primarily for the fact that training is short and the TDL stage only allows the temporal components to be flow through both of which ensure that the learning objective is achieved within a few epochs.

Let $X(t)$ be the input. It is passed through two delayed feeds. Also each of the VRC cell feeds the subsequent cells in each of the layers. As a result capturing of long-term dependencies, tracking time dependent variations etc take place within the auto-encoder. The auto-encoder generates a coded representation of the input patterns which during the decode phase is expanded for use by subsequent layers. Much of the redundancies are discarded in this process. This enables a fast capture of the attributes of the signal and a fine tracking of the variations in the CSI. The auto-encoder layer is shown in Fig. 7. It shows the different constituents and process flow.

At point A, the output is

$$f_{11}(t) = F_{11}\{X_1(t)W_{11}\}, \quad (25)$$
$$f_{12}(t) = F_{12}\{X_1(t-1)W_{12} + f_{11}(t)\}, \quad (26)$$
$$f_{13}(t) = F_{13}\{X_2(t)W_{13} + f_{12}(t)\}, \quad (27)$$
$$f_{14}(t) = F_{14}\{X_2(t-1)W_{14} + f_{13}(t)\}, \quad (28)$$

where $\Sigma_{p=1}^{4} F_{1p}$s are a sequence of VRCs used for processing externally fed $X(t)$ and $X(t-1)$ patterns and $\Sigma_{j=1}^{4} f_{1j}(t)$ internally generated signals scaled by weights W_{1j}.

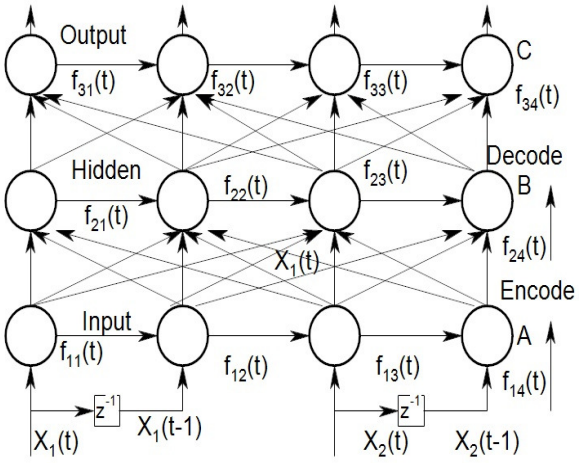

Fig. 7. Different layers of the auto-encoder.

At point B, the output is

$$f_{21}(t) = F_{21}\sum\{f_{11}(t)W_{21i}\}, \quad (29)$$

$$f_{22}(t) = F_{22}\sum\{f_{12}(t)W_{22i} + f_{21}(t)\}, \quad (30)$$

$$f_{23}(t) = F_{23}\sum\{f_{13}(t)W_{23i} + f_{22}(t)\}, \quad (31)$$

$$f_{24}(t) = F_{24}\sum\{f_{14}(t)W_{24i} + f_{23}(t)\}, \quad (32)$$

where $\Sigma_{p=1}^{N}F_{2p}$ are a sequence of VRCs used for processing $f_{2j}(t)$ internally generated signals scaled by weights $\Sigma_{p=1}^{N}W_{2pi}$ for the second layer. Similarly, at point C, the outputs are:

$$f_{31}(t) = F_{31}\sum\{f_{21}(t)W_{31i}\}, \quad (33)$$

$$f_{32}(t) = F_{32}\sum\{f_{22}(t)W_{32i} + f_{31}(t)\}, \quad (34)$$

$$f_{33}(t) = F_{33}\sum\{f_{23}(t)W_{33i} + f_{32}(t)\}, \quad (35)$$

$$f_{34}(t) = F_{34}\sum\{f_{24}(t)W_{34i} + f_{33}(t)\}, \quad (36)$$

where $\Sigma_{p=1}^{N}F_{3p}$ are a sequence of VRCs used for processing $f_{3j}(t)$ internally generated signals scaled by weights $\Sigma_{p=1}^{N}W_{3pi}$ for the third layer. The output of the third layer $Y(t)$ shall take the values of $\Sigma_{p=1}^{4}f_{3p}(t)$.

F. System Model

The system model is constituted by several layers and is applied for generating a close replica of the UAV communication channel. As already discussed, pre-trained layer blocks are added and a number of sets of signals are applied to the system which during the first few cycles only receive an *apriori* reference for carrying a supervised learning. Subsequently the entire process converts to a sequence prediction with the aim of achieving a global objective. The system model of the work is shown in Fig. 8.

The inputs are first applied to the auto-encoder layer. As already discussed, the feature learning, de-noising and context capturing operations are performed by this layer. Simultaneously, the signal is also fed into the recovery layer which uses a combination of TDL-VRC and TDL-LSTM blocks to

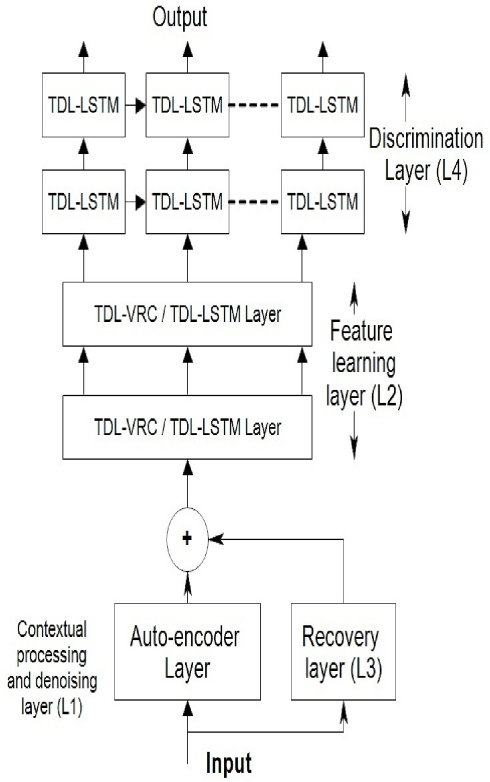

Fig. 8. System model showing different layers.

deal with sparse values and regenerate the lost states of the signal. Such values are received due to high margins of fading or due to poor coverage from the base station. The recovery layer enhances the content richness of the signal. It is mixed with the signal obtained from the auto-encoder layer and is passed on to the temporal modeling layer formed by either TDL-VRC or TDL-LSTM cells. These two different cell types are used to ascertain the effectiveness of the combination. Both have temporal ability and have been found to be effective in capturing long term dependencies present in a signal which is essential in modeling UAV channel. The recovery of the missing components of the signal is done by using a past value of the signal combined with the present state which generates the subsequent version of the input. The combination of TDL-VRC and TDL-LSTM cells in a pack of three compensates nearly all elements of the patterns and regenerates the lost segments of the signal. It ensures that no portion of the input remains unprocessed and extracts a trace which through a regenerative mechanism is expanded into a more effective variant of the signal. The regeneration also restores the characteristics of the patterns which later on contributes towards effective modeling of the UAV channel. The restoration work done by this recovery layer improves after each iteration. During the first iteration the recovery begins with a little gain. As the mechanism sustains, the process exploits the capabilities of the TDL-VRC and TDL-LSTM cells which help the minor trace of the samples to expand.

The layer formed by TDL-VRC and TDL-LSTM cells is called feature learning layer. Two layers are used for the

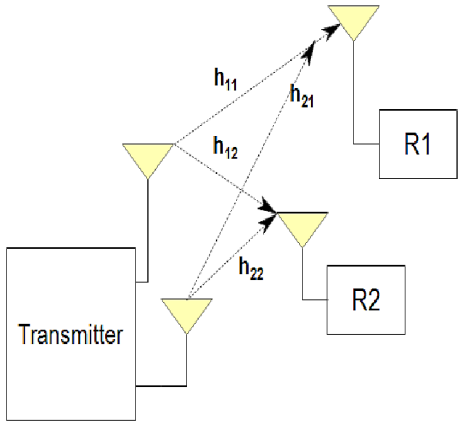

Fig. 9. A generic MIMO block with receivers at different distances.

purpose. One layer feeds the other. Both are of similar length. The two layers help to achieve better learning. Much of the signal reaching this layer is rich in content and free from channel noise to a large extent. Also sparse values are less so nearly no null states of the CSI reaches these two layers. As a result, the learning run is fast and short which is essential for real time situation. The content richness allow the features of the patterns to be learnt appropriately so that the subsequent layer is able to generate the representation of the UAV channel. This section is formed by two layers of the TDL-LSTM cells and is responsible for doing discrimination of different variations of the path-gains of the UAV channel. Here the use of the TDL-LSTM cells ensure that different dependencies of the applied signals are retained, combined with past and present versions of the samples to produce the most relevant variants of the UAV channels CSI states. The TDL-LSTM layers ensure that the complex attributes of all the patterns including temporal, contextual, spatial and historical variations are taken into account while generating the UAV CSI states. The comprehensive learning taking place in this layer is critical not only for the UAV channel path modeling but also for predicting a future version of the CSIs. For a given training window, the system is able to generate an appropriate representation of the UAV channel path gains during each instant of time which is very essential for increasing link reliability and QoS. Initially each of the blocks of the system needs to be trained in a comprehensive manner. The complete system is also trained to achieve the stated objective with prior knowledge applied only during the first few cycles of the training with no pilot carriers required later which provides significant saving of bandwidth under severe fading conditions.

G. Application in a MIMO-NOMA Set-up

The proposed system is configured for application in a NOMA set-up with 2×2 MIMO diversity constituting a MIMO-NOMA arrangement as shown in Fig. 9. Assuming $x_1(i,j)$ and $x_2(i,j)$ be the signals to be transmitted to receivers R_1 and R_2 in a MIMO-NOMA set-up with NLOS channel state. Let R_1 be weak and R_2 be in a strong signal state due to the proximity to the transmitter. Assuming indices i and j related to antenna selection to be known, the transmitted signal is given by

$$y_T(i,j) = P(\sqrt{c_1}x_1(i,j) + \sqrt{c_2}x_2(i,j)), \quad (37)$$

where c_1 and c_2 are power allocation coefficients of the NOMA set-up. As R_1 is at greater distance from the transmitter, $c_1 > c_2$.

At the receiver side, R_1 and R_2 picks up the signal $y_T(i,j)$. The received signals become

$$y_{R_1}(i,j) = y_T(i,j)(h_{11} + h_{12}) + N, \quad (38)$$
$$y_{R_2}(i,j) = y_T(i,j)(h_{21} + h_{22}) + N, \quad (39)$$

with AWGN N.

Assuming MIMO attributes to be incorporated in the definitions (37)–(39), the recovery of $x_1(i,j)$ and $x_2(i,j)$ is done at the receivers. First, R_1 recovers x_1 from y_{R_1}. Due to the far off location of R_1, its power allocation is more as has been already stated. So the recovery of x_1 from y_{R_1} is related to the consideration of x_2 as an interference signal. Using (37) and (38),

$$y_{R_1} = P(\sqrt{c_1}x_1 + \sqrt{c_2}x_2(h_{11} + h_{12}) + N, \quad (40)$$

which after rearranging is written as

$$y_{R_1} = P\sqrt{c_1}x_1(h_{11} + h_{12}) + P\sqrt{c_2}x_2(h_{11} + h_{12}) + N. \quad (41)$$

The second term of (41) is considered to be an interference.

At R_2, successive interference cancelation (SIC) is used to directly recover $x_2(i,j)$. The received signal can be expressed as

$$y_{R_2} = P\sqrt{c_1}x_1(h_{21} + h_{22}) + P\sqrt{c_2}x_2(h_{21} + h_{22}) + N. \quad (42)$$

For both R_1 and R_2, the signal to interference noise ratio (SINR) is expressed as

$$SINR_1 = \frac{Pc_1|h_{11}+h_{12}|^2}{Pc_1|h_{11}+h_{12}|^2+\sigma^2}, \quad (43)$$
$$SINR_2 = \frac{Pc_2|h_{21}+h_{22}|^2}{Pc_2|h_{21}+h_{22}|^2+\sigma^2}, \quad (44)$$

where σ^2 represents noise power. Due to SIC, the x_1 signal is left out making the received signal

$$y'_{R_2} = P\sqrt{c_2}x_2(h_{21} + h_{22}) + N. \quad (45)$$

The received SINR shall be

$$SINR_{2N} = \frac{Pc_2|h_{21}+h_{22}|^2}{\sigma^2}. \quad (46)$$

The data rates achievable at R_1 and R_2 are

$$DR_1 = log_2(1 + SINR_1), \quad (47)$$
$$DR_2 = log_2(1 + SINR_2), \quad (48)$$
$$DR_{2N} = log_2(1 + SINR_{2N}). \quad (49)$$

Here, the channel path gains h_{11}, h_{12}, h_{21}, and h_{22} are determined by the proposed approach discussed above in Section II-F.

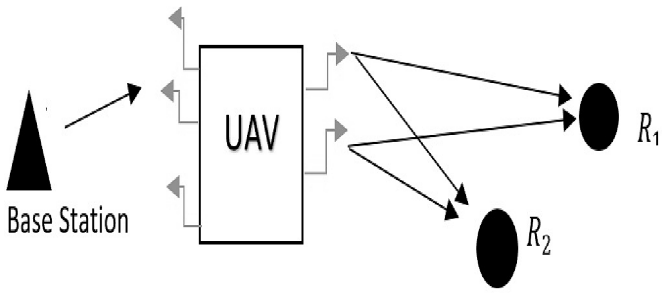

Fig. 10. System set-up with UAV relay node.

H. Application in a MIMO-NOMA Set-up with Energy Harvesting

For efficient operation, drones or UAVs are expected to be of lighter mass so that the power consumption is minimized and as such there is a strict limitation on the battery size or fuel carrying capacity of such vehicles. This in turn limits the range and duration of flight of the aerial vehicle. Small UAVs are practically limited to a flight duration of 20 to 40 minutes [34], on an average. This obstacle can be overcome, if the power supply to the UAV can be taken care of from a remote source through RF EH. With proper EH circuitry, the UAV can gather energy from ambient RF sources or from the signal transmitted to the UAV as part of the communication process by virtue of simultaneous wireless information and power transmission (SWIPT) technology. The harvested energy is essentially consumed for information transmission from the UAV and the residual energy if any may be stored in some energy storage device for future usage. This technique of harvesting the energy required for information transmission can prolong the battery life of the UAV as the stored energy can be completely used for the UAV circuit operation. Most UAVs find application in the form of relay nodes which relays information from a source node to multiple receiver nodes. Once such set up where the UAV acts as a relay node between the base station and the two destination nodes R_1 and R_2, based on the principle of NOMA transmission with a 2×2 MIMO configuration is shown in Fig 10. The base station BS transmits a composite signal x_B, which is a combination of two signals x_1 and x_2, based on the NOMA principle, to the UAV. The signal x_B is given by,

$$x_B(i,j) \quad = \sqrt{P_B}(\sqrt{a_1}x_1 + \sqrt{a_2}x_2). \tag{50}$$

Here $x_1(i,j)$ and $x_2(i,j)$ are the candidate signals for the receivers R_1 and R_1 respectively and a_1 and a_2 are the power allocation coefficients such that $a_1 > a_2$ and $a_1 + a_2 = 1$. The UAV harvests energy from the received signal using time switching protocol. Energy is harvested for a duration of αT with $(0 < \alpha < 1)$ while information processing takes place for the rest of the time frame T i.e., for duration $(1-\alpha)T$. With multiple antenna configuration at the UAV, it is assumed that the UAV considers antenna selection technique to receive the best signal so as to maximize the harvested energy. The signal received at antenna 'n' of the UAV which has channel gain h_{bu_n} with the base station is given by

$$y_B(i,j) = \sqrt{P_B}(\sqrt{a_1}x_1(i,j) + \sqrt{a_2}x_2(i,j))h_{bu_n} + N, \tag{51}$$

where N is AWGN. The energy harvested at the UAV during the first time phase αT is

$$E_h = \eta \alpha T P_B \parallel h_{bu_n} \parallel^2, \tag{52}$$

where η refers to the energy harvesting efficiency and is subjected to the condition that $0 < \eta < 1$. The transmit power available for information transmission over the next phase of time $(1-\alpha)T$ is

$$P_h = \eta \frac{\alpha}{(1-\alpha)} P_B \parallel h_{bu_n} \parallel^2 . \tag{53}$$

Considering decode and forward relaying strategy at the UAV, the UAV decodes the signals x_1 and x_2 from y_B using SIC with the SINR given by $\gamma_{x_1}^U$ and $\gamma_{x_2}^U$ respectively.

$$\gamma_{x_1}^U \quad = \quad \frac{P_B a_1 \parallel h_{bu_n} \parallel^2}{P_B a_2 \parallel h_{bu_n} \parallel^2 + \sigma_0^2}, \tag{54}$$

$$\gamma_{x_2}^U \quad = \quad \frac{P_B a_2 \parallel h_{bu_n} \parallel^2}{\sigma_0^2}, \tag{55}$$

where σ_0^2 is the noise power.

After successful decoding of $x_1(i,j)$ and $x_2(i,j)$, the UAV again forms a composite signal $y_T(i,j)$ to be transmitted to the destinations as a NOMA signal over a MIMO channel as discussed in previous subsection. The SINR available at the receivers R_1 and R_2 to decode $x_1(i,j)$ and $x_2(i,j)$ using SIC can be represented with (43) to (45). The outage of the receivers depends on the successful SIC and decoding of $x_1(i,j)$ and $x_2(i,j)$ at both the UAV and the destinations. Hence the outage probability of signals $x_1(i,j)$ and $x_2(i,j)$ can be written as O_1 and O_2 respectively as

$$O_1 = 1 - Pr\{\gamma_{x_1}^U > \gamma_{th}, \gamma_{x_2}^U > \gamma_{th}\}, \tag{56}$$

$$O_2 = 1 - Pr\{\gamma_{x_1}^U > \gamma_{th}, \gamma_{x_2}^U > \gamma_{th}, \gamma_{x_1}^{R_2} > \gamma_{th}, \gamma_{x_2}^{R_2} > \gamma_{th}\}. \tag{57}$$

Here, γ_{th} is the threshold SNR to declare outage condition.

I. Energy Harvesting Power Management Unit (PMU) for UAV Performance Sustainability

Providing self-sustainability to the UAV communication node is a significant task. For doing so we have designed a highly efficient energy harvesting rectifier and followed by a power management unit (PMU). The rectification unit is responsible to convert the input RF energy into a DC voltage [35] and this DC voltage next passes through the PMU which provides a desired level to the DC voltage and paves the way for its proper storage or direct utilization.

The rectifier designed is derived from the basic idea of a Dickson charge pump. Dickson charge pump is a circuit which is based on the principle of charge multiplication. This simple configuration also works well but when the circuit needs to be modeled in smaller resolution technology, nodes limitation is offered by the drain current as all the dimensions of the device as well as the supply voltage value needs to be scaled to lower values. This has a direct impact on the output current which degrades and as a consequence the power conversion efficiency (PCE) falls. Since transmission gate (TG) can offer a higher current drive and can efficiently transfer both the logic states, the conventional Dickson charge pump is re-configured with

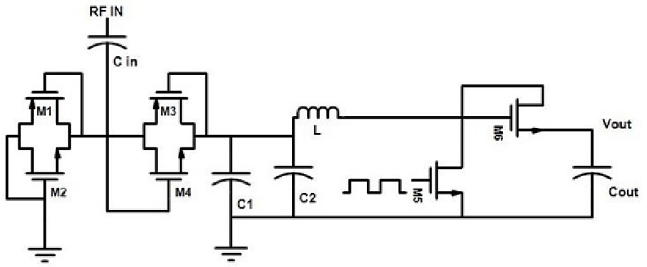

Fig. 11. RF-EH rectifier and PMU.

TG. For a negative cycle the input capacitor will get charged by finding the path through the left side TG (M1-M2) while in the positive cycle the charge in the input capacitor gets transferred to the output capacitor through the TG in the right side (M3-M4) of the schematic. As the current through the TG is high, hence the output power is also high.

In line with the rectifier, to facilitate proper DC output as desired by the specific application we have proposed a simple and modular single stage DC-DC boost converter to achieve desired voltage level to charge a battery. This design is flexible to be operated in multiple ranges of sources from nW to microwatt with a single shared inductor. The proposed power stage has two major features. First, the switching frequency is high because of the adoption of 45 nm technology node. Second, the ripples associated with the inductor current is reduced by more than 80%. The discontinuous mode of operation is performed without having any current sensing mechanism. Fig. 11 shows the basic configuration of a boost converter in line with a RF rectifier where the switch integrated is a metal oxide semiconductor field effect transistor (MOSFET). In our case, the diode has been replaced by a second MOS switch that is essentially used in most of the lower power converters. This implementation helps in extending the battery life of the UAV operations. The experimental details of the design and the output response is discussed below in Section III.

III. Experimental Details and Results

In this section, we discuss the details of the experiments carried out and the results derived.

A. Data

The details of the parameters used for generation of the waveforms is shown in Table I.

The experiments are repeated in a 2×2 MIMO set-up with flat fading and time varying Rayleigh and Rician channel coefficients which are generated using the Jakes model. For 15 numbers of random trials for several cases of Doppler shift, between -10 to 10 dB SNR variations are taken. With both LOS and NLOS components, data block variations between 1000 and 10000, in certain fixed window of timing (60 to 300 s) are taken to produce significant variations in the learning environment. Antenna diversity of all four possible states of the 2×2 MIMO are also taken into account. Further, there is a hardware section consisting of signal generation and testing based on universal software radio peripheral (USRP) sets, spectrum analyzer for viewing and comparing the results, antennas at transmitter and receiver sides (appropriately configured and synchronized). Waveforms of orthogonal frequency division multiplexing (OFDM), 16-quadrature amplitude modulation (QAM) and 64-QAM transmitted in actual field conditions using static and mobile state (using a vehicle with speeds upto 60 Kmph) and received with channel impairments are used to train the system for UAV channel modeling. Using the USRP sets, waveforms are generated with sampling rate of 4 and 8 Mbps, word size of 14 bits per sample, up sampling/ down sampling factor for root raised cosine (RRC) pulse shaping taken to be 16, fast Fourier transform (FFT) size of 256 and cyclic prefix (CP) length of 30. Each transmit frame can carry variable number of OFDM symbols depending on the configuration. Results are obtained using 10 OFDM symbols per OFDM frame. Carrier frequencies considered is 1 GHz. Further, USRP sets (N201 Ettus Research) are placed on top of building structures at around 60 feet above the ground to simulate the height of the UAV while the data recording vehicle is moved at around 60kmph to put the effect of Doppler shift. At one time, either the transmitter or the receiver is mobile as is the case with a UAV. The set-up is used to transmit a 2 s HD video. This segment of the data is used for testing. Using the Jakes model, another set of data have been created for carrier frequencies of 845 MHz, 1.4 GHz, and 2.4 GHz. However, the testing is instantaneous and no timing windows are required. A replica of the waveforms generated for experimental capture of data for training and testing is shown in Fig. 12.

TABLE I
Parameters of combinations used for generation of data for training and testing.

Sl. no.	Item	Parameters
1	Channels types and parameters	Rayleigh and Rician Doppler shift- 30 to 100 Hz SNR- $\pm$10 dB
2	Data block size	1000 to 10,000 chips of 16, 32, 64 bits as inputs
3	Waveform variations	OFDM + 16/32-QAM 256-OFDM, CP of 30 10 OFDM symbols per OFDM frame (USRP) Sampling rate- 4 to 8 Mbps Word size- 14 bits per sample
4	Pulse shaping (USRP)	up/ down sampling with RRC factor of 16 256 FFT, CP of 30
5	Carrier frequency	USRP- 1 GHz Training/ testing data- 845, 1400 and 2400 MHz
6	Window size timings	60 to 300 s
7	Antenna diversity	1×1, 1×2 2×1, 2×2

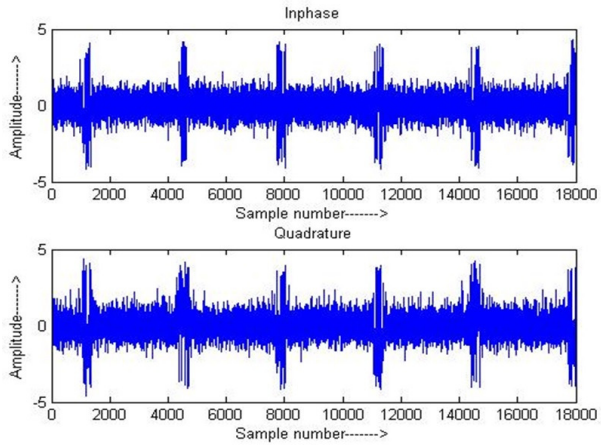

Fig. 12. Waveforms generated for experimental data used during training.

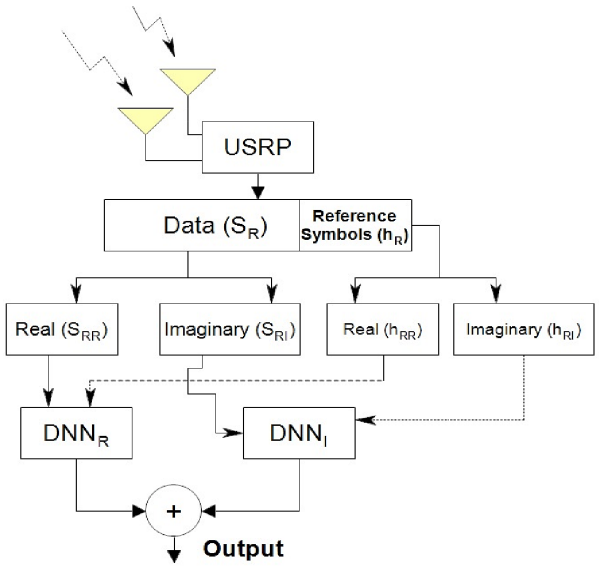

Fig. 13. Experimental set-up showing decoupled DNN blocks for processing real and imaginary components of the waveforms.

TABLE II
PARAMETERS OF DIFFERENT LAYERS OF THE COMPLETE SYSTEM.

Sl. no.	Item	Parameters
1	Overall layers (proposed)	TDL-AE- 1 TDL-LSTM- 2 TDL-VRC- 2 Recovery- 1 Input- 1
	Benchmark	RNN/ NARX- 1 input (Ip), 1 hidden (Hd) 1 output (Op) layers TDNN- 1 Ip, 1 hd, 1 Op layers; two structures one for real and other for imaginary components
2	Max. epochs (pre-train)	TDL-AE =100 TDL-LSTM = 100 Overall = 500
3	Hidden layer length	TDL- AE- Hiden layer length 1.5N, 0.8N, 1.3N TDL-LSTM/VRC- 2 numbers of N length TDL-LSTM- 2 layers of N length; N, input length 16, 32, 64 blocks
4	Criteria for fixing hidden layer	MSE convergence and computational time
5	Weight regularization	0.005
6	Sparsity regularization	2
7	Sparsity proportion	0.05
8	Decoder activation	Purely linear
9	Training	AE- Unsupervised TDL-VRC- SGD BP TDL-LSTM- SGD BP LSTM- SGD BP RNN- BPT TDNN-SGD BP
10	CSI reference block (training)	64, 32, and 16 bit sized repetitions of 10, 8, 6, 4, and 2 blocks

B. Details of Training and Outcomes

Training is the most vital component of the system. A summary of the different parameters related to the proposed model is shown in Table II.

The experimental setup showing decoupled DNN blocks for processing real and imaginary components of the waveforms is shown in Fig. 13. The decoupled blocks adds to the computing cycles but helps in proper recovery of the required contents from the input. Each of the block of the DNN (Fig. 13) has the processing elements of the system as shown in Fig. 8. Each of the layer block (contextual process and de-noising layer, feature learning layer, recovery layer and discrimination layer) are initially trained with supervised SGD BP algorithm. This initial training helps to speed up the learning process of the complete system. In case of the recovery layer, the training of the TDL-VRC and TDL-LSTM layers take place by considering the mean square error (MSE) of each of the cells separately and then taking out an average. The average MSE between the present output (estimate of the pathgain) and the target (reference symbols) is taken as the learning objective. This is because the recovery layer has cells formed by TDL-VRC and TDL-LSTM units. All these layers are initially trained for 100 epochs with *apriori* target feeds incorporated. Except for the recovery layer, the other layers have a size of N (= 16, 32, and 64 depending upon the size of the input). This turnouts to be the size of the received signal block and that way the length of the specific layer is fixed. For the initial cycles, pilot CSI states are applied enabling the system to track a global objective. The prior reference given at the beginning helps to acclimatize the blocks of the system with the expected output. After the acclimatization is over, the system works without reference symbols. The received signal is used as the input to the system while channel path gains are obtained as outputs with the pilot CSIs used as targets. The system is designed and estimate the UAV communications channel path gains.

For each of the blocks, expected output sequences representing the UAV CSI generated using Jakes model and that taken

from actual measurements (as discussed in Section III-C), are available for use in the start-up mode and later during testing. Subsequently, a combination of past and present values produce the future state of the system which in a supervisory learning approach track the changes to reach the desired output. This effort is continued and the complete system is trained with all the available data so that the learning is comprehensive. The diversity in the data helps the learning and also prevents bias states from getting generated. Further, the training cycles are short so that over-training and memorization don't develop and the system strictly executes the action with priority to generalization. The output is a combination of current input and also or previous values, outputs, or states applied and generated from different blocks of the system and finally tracking a global optimal state in which the network attempts to reach the closest to the desired target. After the first cycles of learning, the network reaches a trained state enabling it to generate a sequence like that of a time series which is somewhat similar to that desired from channel modeling. Initially, the system in a training mode tracks the CSI for N time steps which is driven by a least squares (LS) estimation. The system learns CSI of k time steps out of the total acquired N CSI time steps to predict $(k+1)$th CSI in a time step to cover the whole acquired information. In our work, the parameter values for N and k are taken to be between 1000 and 10000 and 8 to 32, respectively.

For each of the blocks,an initial training is carried out assuming 6400 block size with OFDM, 4-QAM, and 8-QAM modulation with signal to noise ratio (SNR) varying between -10 and 10 dB. Upto 100 epochs of the training are sustained with a MSE goal of 10^{-3} taking sub-CSI value block size of 64. The MSE convergence values generated using waveforms with SNR variations reached at certain milestone epochs at different layers are shown in Table III.

Here, as already indicated L1 represents contextual process and denoising layer, L2 feature learning layer, L3 recovery layer and L4 discrimination layer. It is seen that with rise in the SNR value the performance of the training phase improves. This is only an initial training which is required later to shorten the time of learning as a complete system. The presence of the TDL blocks and the differential feeds make the learning faster since it circulates the most relevant portion of the inputs and removes the redundant segments of the signals.

For the feature learning layer, LSTM cells are selected on the basis of MSE convergence recorded upto 1000 epochs as shown in Fig. 14. Both the cells have nearly similar MSE convergence upto 50 epochs but beyond that the LSTM shows better learning. Beyond 500 epochs, the VRC shows no convergence while the MSE curve of the LSTM continues with a downward trend. It indicates that the LSTM cells facilitate better learning. Hence, for experimental purpose, the the feature learning layer is formed by the LSTM cells. After this training is completed, the layers are connected and complete system is trained. For this training, 6400 block size with OFDM, 4-QAM, and 8-QAM modulation with signal varying between -10 and 10 dB passed through 2×2 MIMO channels with Rayleigh and Rician distributions considered. Doppler shift of 30 to 100 Hz have been considered. The

TABLE III
MSE CONVERGENCE FOR DIFFERENT EPOCHS WITH SNR VARIATION IN THE INPUT DATA DEMONSTRATED BY EACH CONSTITUENT BLOCK.

		epochs→				
SNR ↓	Layer	20	40	60	80	100
	L1	0.081	0.073	0.067	0.056	0.031
	L2	0.072	0.061	0.052	0.031	0.02
-5	L3	0.062	0.053	0.041	0.025	0.018
	L4	0.06	0.047	0.038	0.027	0.017
	L1	0.071	0.064	0.051	0.042	0.023
	L2	0.058	0.041	0.032	0.021	0.017
-3	L3	0.057	0.043	0.028	0.02	0.013
	L4	0.055	0.041	0.018	0.012	0.01
	L1	0.061	0.053	0.047	0.036	0.021
	L2	0.052	0.038	0.032	0.018	0.013
-1	L3	0.05	0.03	0.028	0.021	0.011
	L4	0.047	0.027	0.025	0.021	0.010
	L1	0.041	0.033	0.027	0.016	0.005
	L2	0.042	0.031	0.026	0.015	0.004
0	L3	0.04	0.027	0.021	0.016	0.003
	L4	0.037	0.025	0.021	0.015	0.002
	L1	0.037	0.032	0.025	0.015	0.004
	L2	0.032	0.028	0.024	0.011	0.003
1	L3	0.029	0.026	0.02	0.011	0.002
	L4	0.027	0.022	0.019	0.010	0.001
	L1	0.029	0.022	0.015	0.011	0.001
	L2	0.022	0.021	0.020	0.001	0.0008
3	L3	0.021	0.016	0.007	0.006	0.001
	L4	0.02	0.012	0.006	0.004	0.0007
	L1	0.018	0.013	0.011	0.009	0.007
	L2	0.012	0.011	0.009	0.006	0.0002
5	L3	0.011	0.008	0.005	0.003	0.0009
	L4	0.009	0.007	0.002	0.001	0.0004

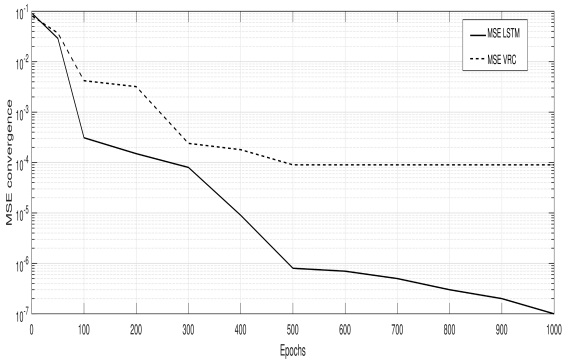

Fig. 14. MSE convergence of LSTM and VRC based layers upto 1000 epcohs.

channel path gains are shown in Fig. 15. The true CSI states of these channel paths are applied as *apriori* knowledge to the system enabling it to learn the patterns. This happens only during the first few cycles of the training where out of 6400 blocks first 10 segments of 64 length sequences are applied as *apriori* labels for four different path gains to the system. It means that the system for the four path gains takes only four instances of the *apriori* CSI states to learn. Subsequently it works on an autonomous mode and starts to generate the path gains as a time sequence. This is recorded with SNR value of 0dB which means that signal elements are not that strengthened.

The block size of the *apriori* CSI used in the training phase is a critical aspect. In the initial phase a few variations of the block sizes are required to ascertain the performance of the

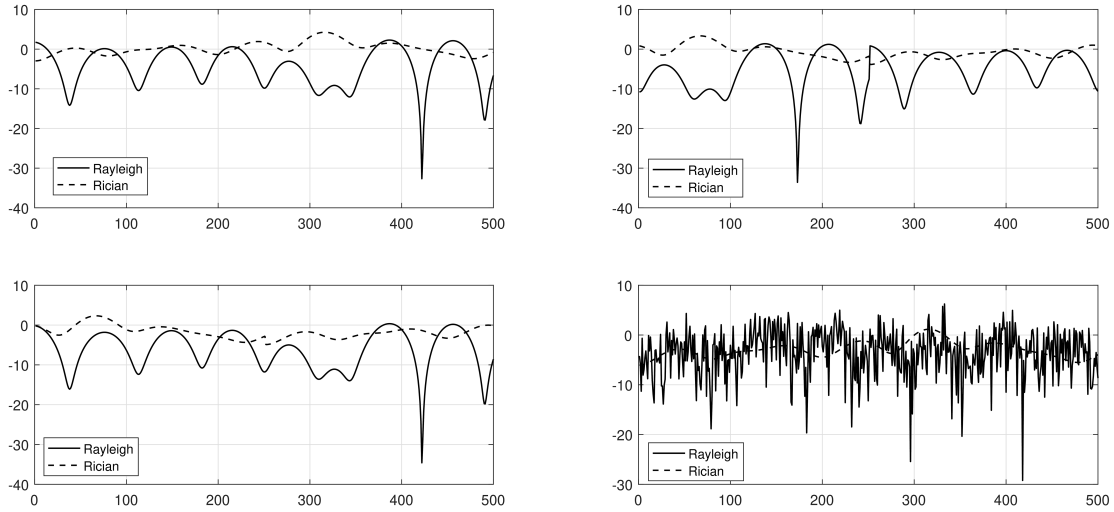

Fig. 15. Path gains of 2 × 2 MIMO channels with Rayleigh and Rician distributions used during training.

TABLE IV
BER VALUES OBTAINED WITH *apriori* CSI BLOCK SIZE AND SNR VARIATION DURING TRAINING.

SNR	Block size			
	10	8	4	2
1	2×10^{-3}	4×10^{-3}	8×10^{-3}	9×10^{-3}
2	0.5×10^{-3}	2×10^{-3}	5×10^{-3}	7×10^{-3}
3	0.2×10^{-3}	0.6×10^{-3}	4×10^{-3}	7×10^{-3}
4	5×10^{-4}	0.1×10^{-3}	4×10^{-3}	7×10^{-3}
5	5×10^{-5}	8×10^{-4}	2×10^{-3}	2×10^{-3}

system. Certain trials are carried out to determine the effect of block sizes in the performance of the system when it is subjected to SNR variations. With block size 10, the network performs best with its discrimination ability enhancing with rise in SNR. Table IV shows BER values obtained with *apriori* CSI block size and SNR variation during training.

C. Effect of L1 and L3 Layers

The roles played by the L1 (contextual process and denoising layer) and L3 (recovery layer) layers are significant. First, a series of experiments are performed to ascertain the role of the L1 layer. Received signals (OFDM modulation passed through Rayleigh faded channel in 2 × 2 antenna diversity) with SNR variation between 0 to 4 dB are applied to the system. First, the SNR variation obtained by using the L1 layer is calculated. Next, the SNR variation due to the absence of the L1 layer is calculated. The system is trained to discriminate between channel paths with all the considered states applied to it before hand. The results obtained are shown in Table VI. It is seen that at 0 dB, the SNR variation between the two cases is 1 dB. Similarly, at 1 dB this margin is 1.39 dB, at 2 dB this gap is 2.3 dB and at 4 dB this difference is 3.25 dB. This clearly indicates that the presence of the L1 layer helps in SNR gain. Therefore it is essential to keep the L1 layer though it adds to the computational complexity which arises only during the training time and is insignificant later.

TABLE V
SNR GAIN DUE TO PRESENCE AND ABSENCE OF L1 LAYER.

Description	SNR in dB				
	0	1	2	3	4
L1 present	1.5 dB	2 dB	3.1 dB	3.65 dB	4.25 dB
L1 absent	0.5 dB	0.61 dB	0.81 dB	0.98 dB	1 dB

TABLE VI
SNR GAIN DUE TO INCREASING % OF NULL STATES IN THE INPUT SEQUENCE.

% of missing data	SNR in dB				
	0	1	2	3	4
0	1.2	1.5	1.8	2.1	2.4
5	1	1.3	1.5	1.7	1.8
10	0.8	1	1.3	1.5	1.6
15	0.6	0.8	0.85	1.1	1.3
20	0.3	0.5	0.6	0.8	1.1
25	0.1	0.2	0.4	0.6	0.8

Another set of experiments are carried out to show the effectiveness of the L3 layer. Here also as done above, in the pre-trained network (with the L1 layer present), the role of the L3 layer is ascertained by reducing the size of the input coming to the system. This is done by continuously incorporating null values between 0 to 25% in gaps of 5%. At 4 dB SNR in the input, the system gives a 1.8 dB gain with 5% missing data. In the worst case, with 25% missing content, the layer helps in attaining a 0.8 dB gain while with 20% null states, the system is able to achieve an addition of 1.1 dB at 4 dB input SNR. This establishes the role played by the L3 layer. It clearly indicates that this layer enhances the performance of the system.

TABLE VII
AVERAGE SNR GAIN GENERATED BY PROPOSED APPROACH COMPARED TO DFE, DDFE, MLP, TDNN, RNN AND NARX.

Set-up	DFE	DDFE	MLP	TDNN	RNN	NARX
1×1	0.67	0.71	0.5	0.4	0.4	0.4
1×1	1.78	1.11	1.1	0.6	0.6	0.6
2×1	2.21	1.16	1.1	0.7	0.8	0.7
2×2	2.6	1.43	1.2	0.8	1.0	0.8

D. Overall Performance

The system is subjected to training using all the pre-trained blocks. It is set to sustain the learning with samples as described above. MSE curves for four situations are recorded. The first MSE is during the training time. Next one is during the testing time. These two curves are generated with the L1 and L3 layers inserted in a pre-trained form. The third and fourth MSE curves are recorded without the L1 and L3 layers, respectively. Fig. 16 shows the four MSE curves. The curves derived without the use of the L1 and L3 layers show that the learning has stopped beyond certain points. Here more number of epochs are not attempted to prevent over training. Some of the common methods used in channel modeling and channel estimation like decision feedback equalizer (DFE) [36], delayed decision feedback estimator (DDFE) [36], and ML approaches like multi layer perceptron (MLP), TDNN, RNN and nonlinear autoregressive exogenous (NARX) are used for comparing the performance of the proposed approach. The calculations are based on MMSE as it is optimal for various structures and data processing techniques. The proposed approach demonstrates significant SNR gain with four different antenna diversity configurations in a Rayleigh faded UAV channel. This is summarized in Table VII. In case of the 2×2 configuration, the proposed approach provides a gain of 2.5 dB over that provided by the DFE based method. For the learning based approaches, this margin is between 0.4 and 1.5 dB. While generating this performance, compared to DFE and DDFE, the present approach required 80% less CSI pilots while for the leaning based approaches like MLP, TDNN, RNN and NARX this margin is around 60%. This is a major advantage of the system.

Table VIII shows the values of capacity (in bit/s/Hz) generated by the proposed approach compared to the theoretical limit and that generated by TDNN, RNN, NARX methods and the technique presented in [37]. The comparisons are done in the LS (time average) and MMSE (ensemble averages) terms. The technique presented in [37] is based on convolutional neural network (CNN) which is effective in vision based pattern recognition problems [8] but requires specific modification in the structure to deal with time varying signals as observed in UAV channels. The results shown in Table VIII are relate to trails carried out using a 2×2 MIMO channel with Rayleigh fading in 60 Hz Doppler. The capacity is linked with the estimation of the path gains. The proposed approach provides content rich path gains which provides average capacity values closer to the theoretical limit.

The proposed approach at 2 dB SNR using LS estimation shows capacity improvement of 0.14 bits/s/Hz compared to RNN, 0.19 bits/s/Hz to that obtained using TDNN and NARX and 0.25 bits/s/Hz using the CNN based technique reported in [37]. While using MMSE, this improvement is 0.09, 0.15, 0.15, and 0.25 bits/s/Hz over those obtained using RNN, TDNN, NARX and [37], respectively. With increasing SNR there is further improvement in the average capacity. This is significant. This improvement has been achieved with only 10% of CSI pilots carriers used during the first cycles of training. As a result, it make huge contribution to bandwidth saving.

The outage performance of the system improves with the MIMO-NOMA set-up where the channel gains are estimated using the proposed approach. The outage performance of the DL assisted MIMO-NOMA set-up is shown in Fig. 17 in comparison to situations where NOMA is not used and MIMO-NOMA is deployed with MMSE based channel path gain estimation. The proposed approach assisted MIMO-NOMA provides near optimal outage performance for an SNR range between -5 and 20 dBm for two users separated by 1 KM distance in Rayleigh fading. The trained system is also used to generate a sequence of path gains of the UAV channel used for generation of the values shown in Table VIII. Fig. 18 shows a representation of the path gain tracking of a MIMO channel with both Rayleigh and Rician distribution. Nearly no parts of the signal are lost which is made possible by the actions of different layers used in the system. The effect of height of the UAV on the outage probability of ground to air (G2A) and air to air (A2A) connections in Rayleigh and Rician fading over a 500 meter radius in studied. The transmission power has a SNR of 20 dB and the height is varied between 10 to 100 meters. The average outage probability of both the channels obtained using the proposed approach is shown in Fig. 19. Outage probability performance improves with greater height. The incorporation of the EH aspects both in terms of channel configuration and device level implementation adds strength to the proposed system. The outage probabilities of the two users at different values of the EH efficiency are plotted in Fig. 20. It clearly indicates that with information transmission using the harvested energy, a proper outage performance can be observed which reassures the fact that the UAV relay node can perform sufficiently well without any dedicated battery source. Hence, an uninterrupted power supply can be guaranteed for information transmission with low outage conditions as opposed to a fixed, vehicle power source which will result in absolute outage once the battery source dries out. Such a system set up uses the CSI to transmit information using NOMA. The required CSI is estimated using the proposed approach.

Further, as reported above (Section II-I), a dedicated block has been implemented to use energy harvesting directly as an aid to extend the UAV battery life. Some of the relevant parameters associated with the design are summarized in Table IX. We have presented a simple, low power, high frequency RF energy harvesting rectifier and a boost converter for specific target storages or applications. It achieves a peak efficiency of 93% at a very low input power of -12 dBm with the use of only six MOSFETs and for smaller value

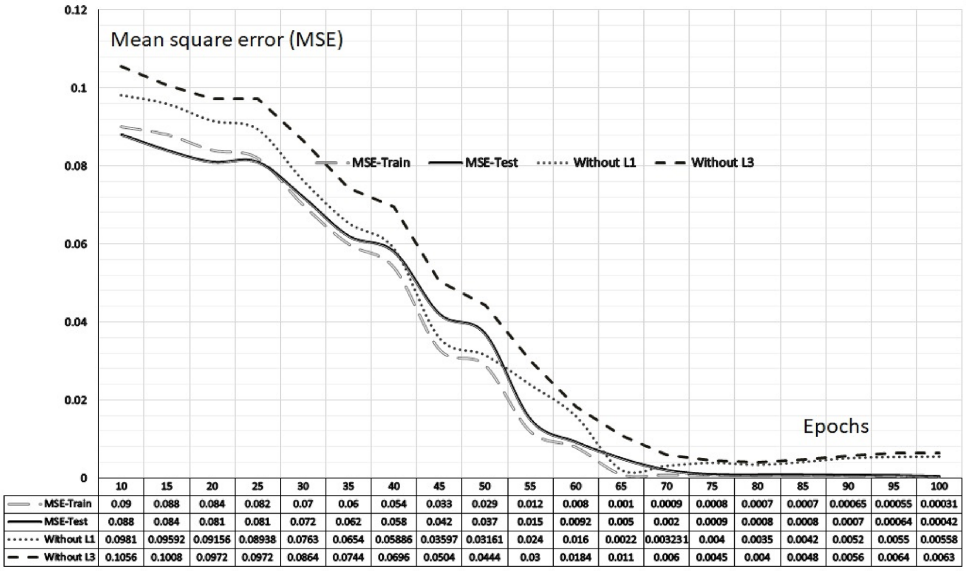

	10	15	20	25	30	35	40	45	50	55	60	65	70	75	80	85	90	95	100
MSE-Train	0.09	0.088	0.084	0.082	0.07	0.06	0.054	0.033	0.029	0.012	0.008	0.001	0.0009	0.0008	0.0007	0.0007	0.00065	0.00055	0.00031
MSE-Test	0.088	0.084	0.081	0.081	0.072	0.062	0.058	0.042	0.037	0.015	0.0092	0.005	0.002	0.0009	0.0008	0.0008	0.0007	0.00064	0.00042
Without L1	0.0981	0.09592	0.09156	0.08938	0.0763	0.0654	0.05886	0.03597	0.03161	0.024	0.016	0.0022	0.003231	0.004	0.0035	0.0042	0.0052	0.0055	0.00558
Without L3	0.1056	0.1008	0.0972	0.0972	0.0864	0.0744	0.0696	0.0504	0.0444	0.03	0.0184	0.011	0.006	0.0045	0.004	0.0048	0.0056	0.0064	0.0063

Fig. 16. MSE v/s epoch plot.

TABLE VIII
AVERAGE CAPACITY GENERATED BY THE PROPOSED SYSTEM COMPARED TO CERTAIN BENCHMARK METHODS.

SNR in dB	LS/MMSE	Capacity (bit/s/Hz)					
		Theory	Proposed	RNN	TDNN	NARX	[37]
2	LS	4.2	4.05	3.91	3.86	3.86	3.8
	MMSE	4.4	4.35	4.26	4.2	4.2	4.1
4	LS	5.6	5.52	5.5	5.5	5.5	4.9
	MMSE	5.8	5.75	5.6	5.6	5.6	5.1
6	LS	7.3	7.26	7.19	7.18	7.18	6.5
	MMSE	7.6	7.54	7.3	7.3	7.3	6.8
8	LS	9.1	9.05	8.94	8.9	8.9	7.2
	MMSE	9.4	9.32	9.25	9.2	9.2	7.8
10	LS	11.6	11.5	11.1	11.1	11.0	7.9
	MMMSE	11.8	11.75	11.5	11.4	11.4	8.1

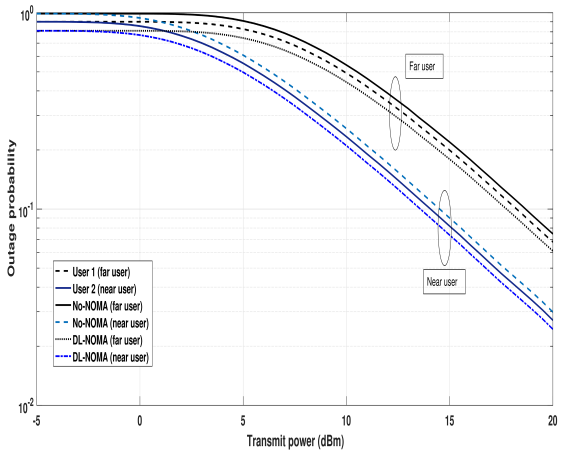

Fig. 17. Outage performance of the MIMO-NOMA system with and without NOMA and proposed approach.

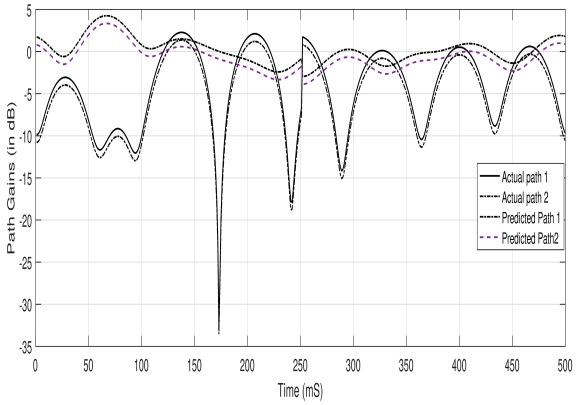

Fig. 18. Actual and tracked path gains.

of inductance which makes the design practically feasible. Moreover it achieves a very good transient settling time of 5.5 s which indicates its capability for high frequency applications. Moreover the design is scalable in the sense that it can be configured for different output voltages as demanded by any target applications. Fig. 21 shows that the system is able to provide 4.9 to 5 V output for input of around 0.8 V which is derived form the received RF signal.

While generating average SNR gain with the 2×2 configuration, by the proposed approach obtains significant performance improvements over DFE and DDFE methods while compared

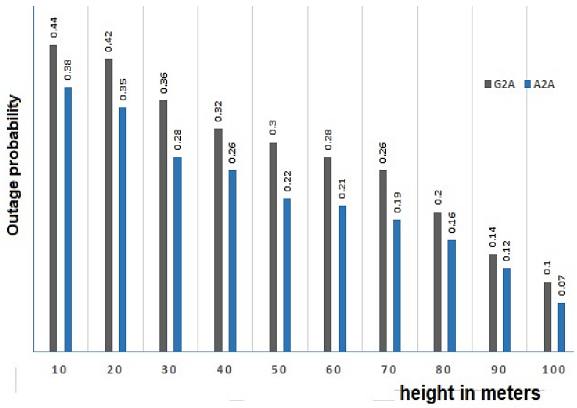

Fig. 19. Average outage probability v/s height of the UAV over a 500 meter radius using a 20 dB SNR OFDM signal.

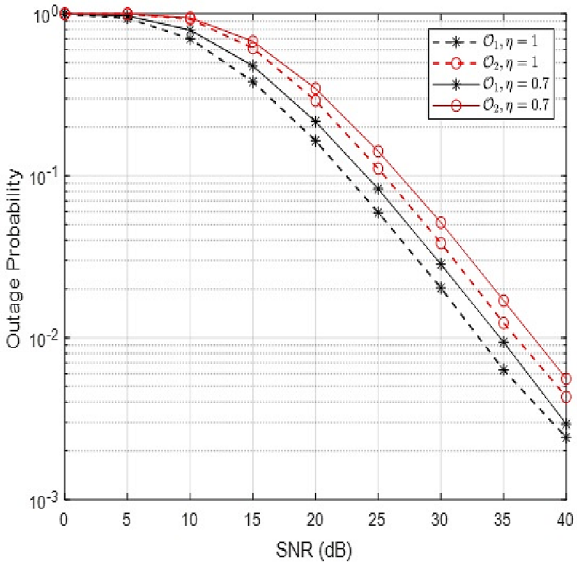

Fig. 20. Outage probability Vs the Transmit SNR for η=[1,0.7].

TABLE IX
PARAMETERS OF DIFFERENT LAYERS OF THE COMPLETE SYSTEM.

Sl. no.	Item	Parameters
1	Technology node	45 nm
2	Input	-12 dBm
3	Output voltage	4.9 V
4	No. of transistors	6
5	Peak efficiency	93%
6	Load transient response	$5.5s@28W$
7	Parameters	Inductor- 10 μH; Capacitor, C_{in}= 100 pF Capacitor, C_{out}= 1 pF Switching frequency= 100 MHz Duty cycle= 90% Input voltage= 800 mV

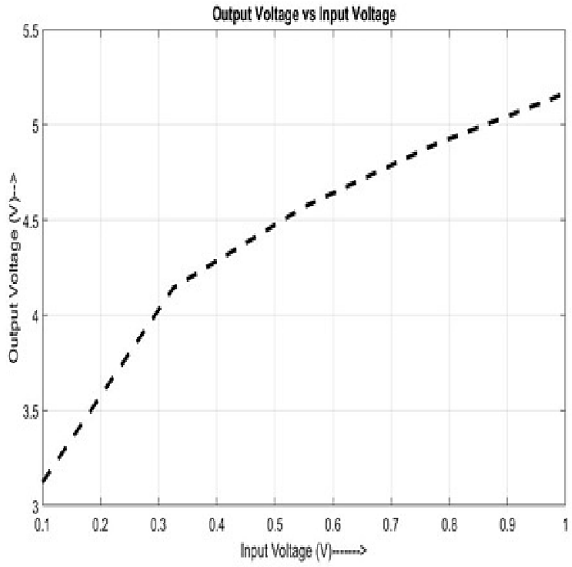

Fig. 21. Output DC voltage across input voltage generated by the RF-EH rectifier and the PMU implemented for battery life extension of the UAV.

to MLP, TDNN, RNN, and NARX, this margins 1.2, 0.8, 1.0, and 0.8 dB, respectively. In obtaining these performances, compared to DFE and DDFE, the present approach takes 80% less CSI pilots while for the leaning based approaches like MLP, TDNN, RNN, and NARX this margin is around 60%. The proposed approach shows capacity improvements with less bandwidth. When the input is 10 dB SNR, the improvements are 1 dB, 1.2 dB, and 1.3 dB compared to TDNN, RNN and NARX respectively obtained with small portion of the CSI pilots carriers taken only during the first cycles of training. As a result, it makes huge contribution towards bandwidth saving. The advantage of the proposed approach is obvious.

IV. CONCLUSION

Here we reported the design of a deep learning based approach formed by gated functions like VRC and LSTM aided by TDL blocks configured for UAV channels. The key parts of the system are contextual process and de-noising layer, feature learning layer, recovery layer and discrimination layer. Extensive training, testing and experiments are carried out using UAV CSI data generated using Jakes model and that taken from actual measurements. The samples cover NLOS and LOS conditions with Doppler shift approximating upto 60 Kmph. Antenna diversity obtained using 2×2 have been used to check the effectiveness of the system to perform in high data rate conditions. The proposed approach shows significant improvements in terms of SNR path gain and capacity (bit/s/Hz) compared to data aided methods like DFE and DDFE and neuro-computing approaches like TDNN, RNN, and NARX. Further, the system has been configured for work with NOMA-MIMO configuration with energy harvesting attributes. System level implementation of RF energy harvesting based PMU to achieve greater battery life has also been incorporated and tested. The system can be very well configured as part of an operational deployment where after the wireless profiling, in the autonomous mode, the UAV communication channel

can be replicated in the best form and wireless links secured for reliable data transfer. With a cloud based CSI capturing arrangement, the knowledge about the channel path gains can be shared among a swarm of drones to build intranets of UAVs which can provide coverage extension to wireless networks.

REFERENCES

[1] K. P. Valavanis and G. J. Vachtsevanos, "UAV applications: Introduction," Handbook of Unmanned Aerial Vehicles, pp 2639–2641, Springer, Dordrecht, 2014.

[2] H. Shakhatreh *et al.*, "Unmanned aerial vehicles: A survey on civil applications and key research challenges," *arXiv preprint arXiv:1805.00881,* 2018.

[3] C. Y.-Banjo and O. Ajayi, "Sky-Farmers: Applications of unmanned aerial vehicles (UAV) in agriculture," *Autonomous Vehicles*, IntechOpen, 2019.

[4] P. Radoglou-Grammatikis, P. Sarigiannidis, T. Lagkas, and I. Moscholios, "A compilation of UAV applications for precision agriculture," *Comput. Netw.*, vol. 172, pp. 1–18, 2020.

[5] J. Farlik, M. Kratky, J. Casar, and V. Stary, " Multispectral detection of commercial unmanned aerial vehicles," *Sensors*, vol. 19, no. 7, pp. 1–28, 2019.

[6] R. Li *et al.*, "Intelligent 5G: When cellular networks meet artificial intelligence," *IEEE Wireless Commun.*, vol. PP, no. 99, pp. 2–10, 2017.

[7] Y.-Y. Chen, Y. Lv, Z. Li, and F.-Y. Wang, "Long short-term memory model for traffic congestion prediction with online open data," in *Proc. IEEE ITSC*, 2016.

[8] I. Goodfellow, Y. Bengio, and A. Courville, "Deep Learning," MIT Press, 2015.

[9] E. Greenberg and P. Levy. "Channel characteristics of UAV to ground links over multipath urban environments," in *Proc. IEEE COMCAS*, 2017.

[10] W. Khawaja, O. Ozdemir, and I. Guvenc. "UAV air-to-ground channel characterization for mmWave systems," *arXiv preprint arXiv:1707.04621,* 2017.

[11] Z. Shi, P. Xia, and Z. Gao, "Modelling of wireless channel between UAV and vessel using the FDTD method," in *Proc. WiCOM*, 2015.

[12] D. W. Matolak and R. Sun, 'AirGround channel characterization for unmanned aircraft systemsPart I: Methods, measurements, and models for over-water settings," *IEEE Trans. Veh. Technol.*, vol. 66, no. 1, pp. 26–44, 2017.

[13] V. Kouhdaragh, F. Verde, G. Gelli, and J. Abouei, "On the application of machine learning to the design of UAV-based 5G radio access networks," *Electronics*, vol. 9, pp. 1–20, 2020.

[14] C. Jiang *et al.*, "Machine learning paradigms for next,-generation wireless networks," *IEEE Wireless Commun.*, vol. 24, pp. 98–105, 2017.

[15] G. Bhutani, "Application of machine-learning based prediction techniques in wireless networks," *Int. J. Commun. Netw. Syst. Sci.*, vol. 7, pp. 131–140, 2014.

[16] R. Cengiz, "Location estimation of base station of mobile phones using artificial neural networks," Master's Thesis, Kadir Has University, Istanbul, Turkey, 2016.

[17] J. N. Foerster, Y.M. Assael, N. de Freitas, and S. Whiteson, "Learning to communicate with deep multi-agent reinforcement learning," *arXiv preprint arXiv:1605.06676,* 2016.

[18] T. Ayoul, T. Buckley and F.Crevier, "UAV navigation above roads using convolutional neural networks," Technical Report, Stanford University, Stanford, CA, USA, 2017.

[19] S. Konam, "Vision-based navigation and deep-learning explanation for autonomy," Master's Thesis, Carnegie Mellon University, Pittsburgh, PA, USA, 2017.

[20] H. Bayerlein, P. D. Kerret, D. Gesbert, "Trajectory optimization for autonomous flying base station via reinforcement learning," in *Proc. IEEE SPAWC*, 2018.

[21] P. V. Klaine, J.P.B. Nadas, R. D. Souza, M. A. Imran, "Distributed drone base station positioning for emergency cellular networks using reinforcement learning," *Cognitive Comput.*, vol. 10, pp. 790–804, 2018.

[22] X. Lu, L. Xiao and C. Dai, "UAV-aided 5G communications with deep reinforcement learning against jamming," *arXiv preprint arXiv:1805.06628,* 2018.

[23] A. V. Makkuva, S, Kannan, S. Oh, and P. Viswanath, "Learning in gated neural networks," *arXiv preprint arXiv:1906.02777,* 2019.

[24] Y. Wu and H. Tan, "Short-term traffic flow forecasting with spatial temporal correlation in a hybrid deep learning framework," *arXiv preprint arXiv:1612.01022,* 2016.

[25] R. Yu, Y. Li, C. Shahabi, U. Demiryurek, and Y. Liu, "Deep learning: A generic approach for extreme condition traffic forecasting," in *Proc. SIAM SDM*, 2017.

[26] Z. Zhao *et al.*, "LSTM network: A deep learning approach for short-term traffic forecast," *IET Intel. Transport Syst.*, vol. 11, no. 2, p. 6875, 2017.

[27] Z. Cui *et al.*, "Deep bidirectional and unidirectional LSTM recurrent neural network for network-wide traffic speed prediction" *arXiv preprint arXiv:1801.02143*, 2018.

[28] Z. Cui, K. Henrickson, R. Ke, and Y. Wang, "HighOrder graph convolutional recurrent neural network: A deep learning framework for network-scale traffic learning and forecasting" *arXiv preprint arXiv:1802.07007*, 2018.

[29] R. Yu, Y. Li, C. Shahabi, U. Demiryurek, and Y. Liu, "Mobility predictions for IoT devices using gated recurrent unit network," *IEEE Internet Things J.*, vol. 7, no. 1, pp. 505–5017, 2020.

[30] H. R. Pamuluri, "Predicting user mobility using deep learning methods," Master Thesis in Computer Science, Blekinge Institute of Technology, Sweden, 2020.

[31] S. Haykin, Digital Communication System, Wiley, New Delhi, $1^{st}ed.$, 2006.

[32] T. Rappaport, Wireless Communications: Principles and Practice, Pearson Education India, New Delhi, 2^{nd} ed., 2010.

[33] l. Bing, "Study on modeling of communication channel of UAV," in *Proc. ICICT*, 2017.

[34] A. M. Le, l. H. Truong, T. V. Quyen, C. V. Nguyen,and M. T. Nguyen, "Wireless power transfer near-field technologies for unmanned aerial vehicles (uavs): A review," *EAI Endorsed Trans. Ind. Netw.*, vol. 7, no. 20, pp. 1–18, 2020.

[35] D. Khan *et al.*, "An efficient reconfigurable RF-DC converter with wide input power range for RF energy harvesting," *IEEE Access*, vol. 8, pp. 79310–79318, 2020.

[36] G. l. Stuber, Mobile Communication, Springer, 2nd ed., New Delhi, 2009.

[37] H. Cheng, S. Ma and H. Lee, "CNN-Based mmWave path loss modeling for fixed wireless access in suburban scenarios," in *IEEE Antennas Wireless Propagation Lett.*, vol. 19, no. 10, pp. 1694–1698, Oct. 2020.

[38] F. Erden, C. K. Anjinappa, E. Ozturk, and I. Guvenc, "Outdoor mmwave base station placement: A multi-armed bandit learning approach," *arXiv preprint arXiv:2003.03494,* 2020.

[39] A. H. Arani, M. M. Azari, W. Melek, and S. Safavi-Naeini, "Learning in the sky: An efficient 3D placement of UAVs," *arXiv preprint arXiv:2003.02650,* 2020.

Aradhana Misra is currently working as Assistant Professor in the Department of Electronics and Communication Engineering, Gauhati University in Guwahati, Assam. She is specialized in the area of Signal processing and Wireless Communication with focus on physical layer technologies for 5G and beyond networks. She obtained her Ph.D (2021) from Gauhati University, India in the area of Wireless communication, M. Tech (2011) in Electronics and Communication Technology from Gauhati University and B.Tech (2007) in Electronics and Communication Engineering from Sikkim Manipal Institute of Technology, Gangtok, India.

Manash Pratim Sarma is currently working as Assistant Professor in the Department of Electronics and Communication Engineering, Gauhati University, Assam, India. He has obtained M.Sc degree in Electronics from Gauhati University, India and M.Tech degree in Electronics Design and Technology from Tezpur University, Assam, India. His research interest includes VLSI, High speed VLSI design for communications, CMOS circuit design etc.

Kandarpa Kumar Sarma (Senior Member, IEEE) received the M.Tech. degree in Signal Processing from IIT Guwahati, India, in 2005, and the Ph.D. degree from the Department of Electronics and Electrical Engineering, IIT Guwahati. He is currently with the Department of Electronics and Communication Engineering, Gauhati University, India, as a Professor and the Head. He has authored ten books and several research articles. His research interests include applications of deep learning and soft-computational tools, cognitive radio, electronic warfare, mobile communication, pattern recognition, and language technology. He is also a Fellow of IETE, India.

Nikos E. Mastorakis (Senior Member, IEEE) received the B.Sc. (Ptychion) degree in Pure Mathematics, the B.Sc. and M.Sc. (Diploma) degrees in Electrical Engineering, and the Ph.D. degree in Electrical Engineering and Computer Science from the National University of Athens, Greece. He also studied medicine at the Medical School of Athens, National University of Athens. He had served as a Special Scientist on computers and electronics in the Hellenic (Greek) Army General Staff from 1993 to 1994 and taught several courses for the Department of Electrical and Computer Engineering, National Technical University of Athens, from 1994 to 1998. He was a Visiting Professor with the School of Engineering, University of Exeter, U.K., in 1998, and a Visiting Professor with the Technical University of Sofia, Bulgaria, from 2003 to 2004. He is currently a Professor with the Technical University of Sofia and the Department of Computer Science, Military Institutions, University Education (MIUE)Hellenic Naval Academy, Greece. He was the first that solved with several different approaches to the former unsolved problem of multivariable factorization and published it. He was also the first scholar that completely solved the problem of stability for multidimensional systems using genetic algorithms. It was the first that constructed electronic musical instrument with the spaces of the Byzantine music. He is an Active Researcher in applied mathematics and computer science (systems theory, control, optimization theory, algorithms theory, signal processing, robotics, and computational intelligence). He has edited more than 200 books and authored five books. He has published more than 600 articles in international books, journals, and conferences. He is also a member of the New York Academy of Sciences, the A. F. Communications and Electronics Association, the American Association for the Advancement of Science, and other smaller scientific societies. He is also an active reviewer of 26 international journals, a member of the Editorial Board of 13 international journals, and an Editor of International Book Series: Editor of the series Electrical and Computer Engineering (WSEAS Press) and Editor of the series Mathematics and Computers in Science and Engineering (WSEAS Press). He is also a member of the Editorial Board of Advances in Computation: Theory and Practice (NOVA). He received several awards, including the Royal Society of England and the Hellenic National Research Foundation, for his academic studies and his scientific research. He is the Editor-in-Chief in many international journals. He was the General Chairman in more than 30 international conferences. He has organized more than 40 special sessions and three workshops and has given many plenary lectures. He is a registered Professional Electrical and Mechanical Engineer. He also received the Prize of Excellence from the Romanian Academy of Science, Bucharest, Romania.